1-1-2019

Theoretical Investigation on The Single Transition-Metal Atom-Decorated Defective MoS2 for Electrocatalytic Ammonia Synthesis

Haoran Guo
University of Electronic Science and Technology of China, Ningbo Institute of Materials Technology and Engineering, University of Chinese Academy of Sciences

Lei Li
University of Electronic Science and Technology of China, Ningbo Institute of Materials Technology and Engineering, University of Chinese Academy of Sciences

Xingyong Wang
University of Wollongong, xingyong@uow.edu.au

Ge Yao
Nanjing University

Haibo Yu
University of Wollongong, hyu@uow.edu.au

See next page for additional authors

Publication Details Citation

Guo, H., Li, L., Wang, X., Yao, G., Yu, H., Tian, Z., Li, B., & Chen, L. (2019). Theoretical Investigation on The Single Transition-Metal Atom-Decorated Defective MoS2 for Electrocatalytic Ammonia Synthesis. Faculty of Science, Medicine and Health - Papers: Part B. Retrieved from https://ro.uow.edu.au/smhpapers1/936

Theoretical Investigation on The Single Transition-Metal Atom-Decorated Defective MoS2 for Electrocatalytic Ammonia Synthesis

Abstract

Using density functional theory (DFT) calculations, we explored the potential of defective MoS2 sheets decorated with a series of single transition metal (TM) atoms as electrocatalysts for N2 reduction reaction (NRR). The computed reaction free energy profiles reveal that the introduction of embedded single TM atoms significantly reduces the difficulty to break the N≡N triple bond, and thus facilitates the activation of inert nitrogen. Onset potential close to -0.6 V could be achieved by anchoring various transition metals, such as Sc, Ti, Cu, Hf, Pt, and Zr, and the formation of the second ammonia molecule limits the overall process. Ti-decorated nanosheet possesses the lowest free energy change of -0.63 eV for the potential determining step. To better predict the catalysis performance, we introduced a descriptor, φ, which is the product of the number of valence electron multiplying by the electronegativity of the decorated TM. It shows good linear relationship between the d-band center and the binding energy of nitrogen, except for those metals with less than half filled d-band. Although the metals in Group IIIB and IVB have strong adsorption interactions with N atom, the Gibbs free energy changes for desorption of the second ammonia are unexpectedly low. The selectivity of these systems towards nitrogen reduction reaction (NRR) are also significantly improved. Therefore, those defective MoS2 decorated with Sc, Ti, Zr and Hf are suggested as promising electrocatalysts for NRR, for their both high efficiency and selectivity.

Keywords

single, synthesis, ammonia, electrocatalytic, mos2, defective, investigation, theoretical, transition-metal, atom-decorated

Publication Details

Guo, H., Li, L., Wang, X., Yao, G., Yu, H., Tian, Z., Li, B. & Chen, L. (2019). Theoretical Investigation on The Single Transition-Metal Atom-Decorated Defective MoS2 for Electrocatalytic Ammonia Synthesis. ACS Applied Materials and Interfaces, 11 36506-36514.

Authors

Haoran Guo, Lei Li, Xingyong Wang, Ge Yao, Haibo Yu, Ziqi Tian, Baihai Li, and Liang Chen

Theoretical Investigation on The Single Transition Metal Atom Decorated Defective MoS_2 for Electrocatalytic Ammonia Synthesis

Haoran Guo,[1,2,3,#] Lei Li,[1,2,3,#] Xingyong Wang,[4] Ge Yao,[5] Haibo Yu,[4] Ziqi Tian,[2,3,6,*] Baihai Li,[1,*] Liang Chen[2,3,*]

[1]School of Materials and Energy, University of Electronic Science and Technology of China, Chengdu 611731, Sichuan, China.

[2]Ningbo Institute of Materials Technology and Engineering, Chinese Academy of Sciences, Ningbo 315201, Zhejiang, China.

[3]University of Chinese Academy of Sciences, 100049, Beijing, China.

[4]School of Chemistry and Molecular Bioscience, Molecular Horizons, University of Wollongong, Wollongong, NSW 2522, Australia

[5]School of Physics, Collaborative Innovation Center of Advanced Microstructures, and National Laboratory of Solid State Microstructures, Nanjing University, Nanjing 210093, Jiangsu, China.

[6]Fujian Institute of Innovation, Chinese Academy of Sciences, Chinese Academy of Sciences, Fuzhou, Fujian, 350002, P.R. China.

E-mail: tianziqi@nimte.ac.cn

E-mail: chenliang@nimte.ac.cn

E-mail: libaihai@uestc.edu.cn

Abstract

Using density functional theory (DFT) calculations, we explored the potential of defective MoS_2 sheets decorated with a series of single transition metal (TM) atoms as electrocatalysts for N_2 reduction reaction (NRR). The computed reaction free energy profiles reveal that the introduction of embedded single TM atoms significantly reduces the difficulty to break the N≡N triple bond, and thus facilitates the activation of inert nitrogen. Onset potential close to -0.6 V could be achieved by anchoring various transition metals, such as Sc, Ti, Cu, Hf, Pt, and Zr, and the formation of the second ammonia molecule limits the overall process. Ti-decorated nanosheet possesses the lowest free energy change of -0.63 eV for the potential determining step. To better predict the catalysis performance, we introduced a descriptor, φ, which is the product of the number of valence electron multiplying by the electronegativity of the decorated TM. It shows good linear relationship between the *d*-band center and the binding energy of nitrogen, except for those metals with less than half filled *d*-band. Although the metals in Group IIIB and IVB have strong adsorption interactions with N atom, the Gibbs free energy changes for desorption of the second ammonia are unexpectedly low. The selectivity of these systems towards nitrogen reduction reaction (NRR) are also significantly improved. Therefore, those defective MoS_2 decorated with Sc, Ti, Zr and Hf are suggested as promising electrocatalysts for NRR, for their both high efficiency and selectivity.

Keywords: Density functional theory; Nitrogen reduction reaction; Single atom catalysts; Electrocatalysis; MoS_2

Introduction

Large-scale artificial nitrogen fixation, also known as the Haber-Bosch process, is one of the most important discoveries in the twentieth century.[1-2] Synthesized ammonia (NH_3) is mainly used for the production of fertilizers that support the rapid growth of global population.[3] To date, global NH_3 production is over 150 million tons per year, 80% of which is further used in the production of fertilizers to feed one-third to half of the world population. Moreover, due to its portability and high energy density, NH_3 is also supposed to be an attractive carbon-free energy carrier in the future.[4-5] Because of the inert triple bond with bond energy of 940.95 $kJ \cdot mol^{-1}$ in the N_2 molecule, the current ammonia production process requires high pressure (150~350 atm) as well as high temperature (350~550 °C). Over 1% of global energy consumption goes to ammonia production, resulting in huge amount of CO_2 emission. Electrochemical N_2 reduction reaction (NRR) is a state-of-the-art technology that supplies an energy-saving alternative for artificial N_2 fixation.[6-7] NH_3 is yielded through a 6-electron process coupled with proton transfers ($N_2+6H^++6e^-\rightarrow 2NH_3$). The renewable energy sources, such as solar and wind, can be utilized to power this reaction, making the NH_3 production more environmentally benign. Despite great efforts being made both experimentally[8-17] and theoretically,[18-30] it still remains a challenge to discover an active, selective and efficient electrocatalyst for industrial application.

Recently, single-atom catalysts (SACs), of which single transition metal (TM) atoms are dispersed on a substrate as the active center, have been becoming a rising star in heterogeneous catalysis.[31] The highly under-coordinated sites can be more active than the surface of bulk materials. Besides, one can tune the intrinsic activity by altering the substrate environment.[32-33] SACs have been applied in a variety of electrocatalysis processes, including hydrogen evolution reaction (HER),[34-35] oxygen reduction reaction (ORR),[36-38] oxygen evolution reaction (OER),[39-40] and NRR.[41] Owing to the large surface area and novel electronic properties, two-dimensional (2D) materials are widely used as the substrates for the fabrication of SACs,[42-43] such as the graphene-like single-layered molybdenum disulfide (MoS_2). Azofra *et al.* suggested that single atom Fe

deposited on MoS_2 monolayer exhibits high selectivity towards N_2 reduction against chemisorption of CO_2 and H_2O.[44] In addition, we have previously demonstrated that the edge of MoS_2 layer and the defect-rich MoS_2 nanostructures with the low Gibbs free energy changes of 0.68 and 0.60 eV for the PDS steps on the respective NRR free-energy profiles were promising for NRR catalysis.[15-16] However, although the under-coordinated Mo site can effectively activate the inert N_2 molecule, desorption of NH_3 is energetically unfavorable. For the edge and defect, the Gibbs free energy changes of NH_3 desorption are 0.90 and 0.87 eV, respectively. Ling[45] and Wang[46] *et al* revealed that B/g-C_3N_4 and Mo/C_2N might be potential candidates of single atom catalysts for NRR with the rather low onset overpotential of 0.20 and 0.17 V, respectively. However, the Gibbs energy changes for desorption of the first NH_3 molecule on the energy profiles of NRR process were not clarified. Furthermore, some other investigations demonstrated that the under-coordinated Mo site is quite active and may initiate the undesirable HER reactions which is competing with NRR process.[47-48] Herein we notice that the defective MoS_2 may be a potential substrate to hold the single transition metal atoms. Are these SACs still effective in N_2 activation? Can the selectivity be improved via anchoring single TM atoms on the defect of single-layered MoS_2?

To answer these questions, we performed density functional theory (DFT) calculations to investigate a series of transition-metal decorated defective MoS_2 nanosheets. The metal elements from IIIB to IIB subgroups except Tc and Hg were chosen as the candidates, which were embedded into the nanosheet with a MoS_2 formula vacancy. The potential performance on NRR catalysis was evaluated based on free energy calculations. Our calculations indicate that the addition of electron-proton pair to *NH or *NH_2 is the potential determining step (PDS) for all the SACs. The defective MoS_2 decorated with Sc, Ti, Cu, Hf, or Zr are suggested to be good candidates for N_2 reduction to NH_3, with the energy changes of PDS lower than 0.7 eV. Furthermore, we proposed an empirical descriptor to predict the properties of SACs, which correlates with the *d*-band center and N-binding energy very well. It is indicated that transition metals with less than half filled *d*-band, such as Sc and Ti, do not follow

the linear scaling relationship.[49] Catalysts containing these single atoms may be able to overcome the limitation governed by the relation.

Computational details

The spin-polarized density functional theory (DFT) computations were carried out by using Vienna ab initio software package (VASP).[50-53] The electron exchange-correlation interactions were treated within the generalized gradient approximation (GGA) in the form of the Perdew-Burke-Ernzerhof (PBE) functional.[54] The Projector Augmented Wave (PAW) potentials were used for description of the core electrons.[55] Van der Waals interactions were considered using DFT-D3 correction.[56] Slab model was constructed based on a 5×5×1 supercell of MoS_2 single layer to simulate a relatively low density of defect, with a vacuum of 20 Å along the z-direction. One Mo atom with two neighboring S atoms were removed from the perfect sheet as the defect. A single TM atom was located in the vacancy as the active site. All the 3*d*, 4*d*, 5*d* transition metals except Tc, Hg and lanthanide were screened to search for the potential candidates. A 2×2×1 Monkhorst-Pack[57] k-point sampling was used for the geometry optimization. Energy cut-off of plane wave was set to 450 eV. The threshold of geometry optimization was set to 0.005 eV•$Å^{-1}$ in force on each atom. All the atoms within the box were fully optimized without any constraint.

Gibbs free energy change (ΔG) was evaluated based on the computational hydrogen electrode (CHE) model,[18] which takes one-half of the chemical potential of gaseous hydrogen under standard conditions as the free energy of the proton-electron pairs. ΔG were calculated by the following equation:

$$\Delta G = \Delta E + \Delta E_{ZPE} - T\Delta S - neU + \Delta G_{pH} \quad (1)$$

where ΔE, ΔE_{ZPE}, ΔS are the reaction energy from DFT calculation, the correction of zero-point energy and the change of simulated entropy, respectively. T is the temperature (T = 298.15 K). *n* and U are the number of transferred electrons and the

applied potential, respectively. The calculated values of ΔE_{ZPE} and $T\Delta S$ are listed in **Table S1**. ΔG_{pH} is the correction on the pH in the electrolyte that equals to kT×ln10×pH. Since in experiment hydrochloric acid with a concentration of 1 mol/L is often used as the electrolyte, this term can be considered as 0.

Result and discussion

All the decorated MoS_2 nanosheets have quite similar structures after relaxation. The optimized structure of the Sc-decorated defective MoS_2 sheet was shown in **Figure 1**, and the coordinates of the Sc-based SAC and the intermediates of NRR on the SAC were shown in the end of Supporting Information as a typical example. The TM-sulfur bond lengths of all the investigated systems range from 2.10 to 2.60 Å, indicating that TMs are embedded into the defect via chemical bonding. The pristine MoS_2 sheet is a semiconductor, while these TM-decorated systems exhibit good electrical conductivity (**Figure S1**). Therefore, introducing TM single atoms at the defect could improve the material's conductivity, which may be used as a better electrocatalyst. Zhao *et al.*[58] have theoretically investigated another kind of decorated MoS_2 nanosheets with one S atom removed and a single TM atom deposited at the vacancy. They predicted that replacing one S atom by a neutral metal atom could dramatically increase the catalytic activity, and the Mo-embedded nanosheet is the most promising one with an onset potential of -0.53 V. Based on our previous experience combined both experiment and theoretical studies on the defective MoS_2,[16] we removed one neutral MoS_2 unit and deposited a single TM metal atom at the defect to construct the SAC model. It is believed that the TM atom coordinated with 4 neighboring S atoms should be stable. To evaluate the possibility of SAC formation, we calculated the formation energy, E_{form}, by the following formula:

$$E_{form} = E_{total} - E_{MoS2} + \mu_{Mo} + 2\mu_S - \mu_{TM} \quad (2)$$

where E_{tatal} and E_{MoS2} represent the energies of the single metal atom decorated defective MoS_2, the 5×5 supercell MoS_2 layer, respectively. μ_{Mo}, μ_S and μ_{TM} are the

chemical potentials of Mo, S and TM atom, respectively. As listed in **Table S2**, the metals in group IIIB and IVB have the lowest formation energies, ranging from 5.11 to 5.97 eV. Interestingly, our calculated values are comparable with the formation energies of 5.15 eV for two S vacancies, and lower than that of 6.93 eV for a Mo vacancy formed in the pristine MoS_2, respectively, as reported by Santosh *et al.*.[59] The results imply that deposition of a TM atom at the defect of MoS_2 will not induce additional energy consumption than that for creating two S vacancies and even save the energy to remove a Mo atom from MoS_2 monolayer, suggesting that these TM decorated structures should be feasible for synthesis. *Ab initio* molecular dynamics (AIMD) simulations were performed at 500K to confirm the thermodynamic stability of the decorated structures, which evidenced that the configuration has no significant distortion in 10 ps, as shown in **Figure 2**. Thus, such decorated systems should be very stable at ambient condition.

Considering the different N_2 adsorption sites and hydrogenation sequences, the NRR process has three possible reaction pathways, known as distal, alternating and enzymatic paths (Scheme 1).[23] In all these three mechanisms, six proton-electron pairs (H^++e^-) are added one by one to the N_2 molecule. For the distal mechanism, first three proton-electron pairs are added to the terminal N atom, resulting in the cleavage of N-N bond and the generation of the first NH_3 molecule. Then the following three protonation steps take place on the other N atom bonding to the SAC. In comparison, hydrogenations occur alternately between two N atoms in the alternating mechanism. As a result, two NH_3 molecules are released successively. In addition, enzymatic mechanism has also been discussed in recent studies,[20, 23, 26] in which N_2 molecule is adsorbed via the side-on rather than end-on mode. Both two nitrogen atoms form bonds with active sites in subsequent steps. Besides, a hybrid mechanism may exist in which some species shuttle from one pathway to another one.

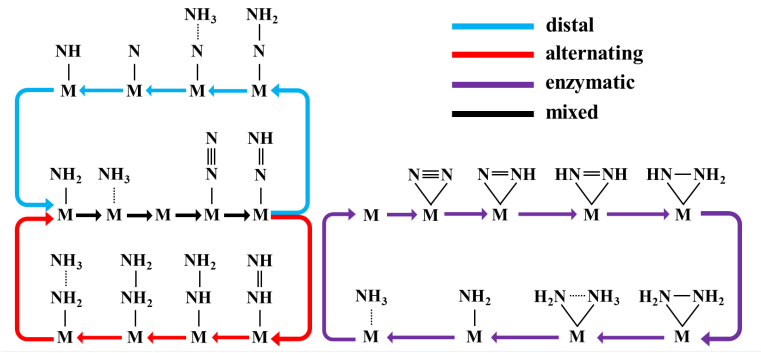

Scheme 1. Schematic illustration of the three mechanisms for NRR: distal, alternating and enzymatic mechanisms. M stands for the TM atom.

Based on the aforementioned mechanisms, we screened a series of TM atoms decorated at the defect of MoS_2. Free energy profiles of the whole reaction pathways have been explored. For all these SACs systems, the free energy changes have similar trends that the distal mechanism is energetically preferential, while the formation and desorption of the second ammonia molecule limits the overall reaction (**Figure 3**). Namely, the step of *NH→*NH_2 or *NH_2→*NH_3 determines the overpotential of NRR. According to the heights of the potential determining step (PDS), we classified the studied elements into three groups which have the highest free energy changes under 0.70 eV, between 0.70 to 1.00 eV, and above 1.00 eV. Those elements with energy increases under 0.70 eV, such as Sc, Ti, Cu, Zr, Hf, and Pt, are proposed to be promising candidates for application, and taken as typical systems for further discussion. Their free energy profiles are plotted in **Figure 3**. For clarity, the free energy diagrams for other elements are depicted in **Figure S2**. In order to evaluate the influences of solvation on the adsorption energies of the intermediates and the free energy diagrams of NRR process, the polarizable continuum models (PCM)[60-61] was used to simulate the solvation effect. The calculated results indicate that the solvation has different contributions to the energies of the intermediates, e.g., the solvation energies of 0.08 and -0.46 eV for *NNH and *NNH_3 on Sc-based electrocatalyst, respectively. As a result, the free energy diagrams were changed as well, as shown in **Figure S3**. Generally, the energy changes of the PDS step on the distal NRR mechanism were reduced. For example, the values were reduced from 0.67 and 0.63 eV to 0.54 and 0.56 eV for Sc

and Ti-based SACs, respectively.

Due to the high stability of the triple bond, the activation of N_2 molecule is usually difficult at ambient condition. The first hydrogenation step of the physisorbed N_2 ($*N_2 \rightarrow *NNH$) occurring on the bulk material surface is supposed to be the PDS.[18] In contrast, the single atom embedded in the 2D substrate is able to polarize inert N_2 molecule, and then weaken the triple bond. The charge density difference of valence band maximum (VBM) at surface metal plane for the optimized Sc-decorated MoS_2 was visualized in **Figure 1**. The electrons clearly accumulate at the hollow site formed between Sc atom and two defective Mo atoms, which may polarize and then activate the inert N_2 molecule. It is so active that the binding between N_2 and Sc atom is considerably strengthened, leading addition of the first (H^++e^-) pair to be feasible. As for the decorated MoS_2 monolayers with Sc, Ti, Zr and Hf, N_2 can be chemisorbed on the single transition metal atoms with the N-TM bond lengths less than 3 Å. The N-containing species on Sc-based SAC were shown in **Figure 4**. Both N atoms in each of the $*N_2$, *NNH and $*NNH_2$ configurations might interact with the anchored TM atoms. For instance, the distances between Sc and two N atoms in the $*N_2$ configuration are 2.23 and 2.46 Å, respectively. We speculate that the nitrogen fixation on this kind of SAC may proceed via a hybrid mechanism combining the distal and enzymatic processes rather than the pure distal path. From $*N_2$ to *N in all the SAC systems, the steps are either exothermic or with moderate energy changes of lower than 0.40 eV, leading to facile formation of the first ammonia molecule.

On the other hand, the intermediate *N on all the pathways are relatively stable. The nitrogen is tightly binding to the single metal atom, resulting in the positive ΔG for formation of the second ammonia. The energy changes of PDS on the NRR pathways are 0.67, 0.63, 0.66, 0.69, 0.67 and 0.68 eV for Sc, Ti, Cu, Zr, Hf and Pt, respectively. The values are lower than the results reported in our previous work, in which nitrogen reduction takes place at the edge or vacancy of MoS_2 monolayer.[15-16] In the cases of Sc, Ti and Zr, NH_3 desorption needs to overcome an even higher energy changes (0.68 ~ 0.72 eV). This step involves no electron transfer, having thus no influence on the

overpotential of NRR.

The free energy diagrams for the screened metals indicate that the reductive hydrogenation of the second nitrogen limits the overall catalytic performance. As listed in **Table 1**, the elements with relatively low energy changes of PDS are all in Group IIIB, IVB, VIIIB and IB, especially in Group IVB. In contrast, the energy changes of PDS for elements in Group VB, VIB and VIIB are all higher than 1.00 eV. The PDS occurs at either *NH→*NH_2 or *NH_2→*NH_3 step, implying that the binding between the second nitrogen and the single metal atom is too strong to facilitate desorption of NH_3 from the electrode. Previous studies suggested that the binding energy of nitrogen, E_b(N), is an effective descriptor to predict the NRR performance.[18] Consistently, our calculations also indicate that the formation and desorption of the second NH_3 becoming the limiting factor of the overall reaction is a result of the high stability of the intermediate *N. The interactions between the *d*-orbitals of the metal and the *p*-orbitals of nitrogen are responsible for the formation of *N, thus the *d*-band center, ε_d, is assumed to be in connection with the strength of binding interaction. Interestingly, the E_b(N) has an approximately linear relationship as a function of the ε_d of the single TM atoms, as shown in **Figure 5(a)** (see **Table S3** for details). Higher ε_d is related to more negative E_b(N), and stronger nitrogen-metal interactions. To achieve a high NRR activity, metals with low ε_d values are recommended, such as Cu and Pt.

Recently, Rossmeisl and Koper *et al.*[62-65] revealed that the linear relations between number of electrons and adsorption energies and its influences on the electrocatalytic activities of metals, oxides, and SACs. Xu *et al*.[33] introduced a descriptor by combining ab initio calculations with empirical parameters to predict the OER/ORR/HER activities of graphene-based SACs. Inspired by their work, we proposed a similar descriptor, φ:

$$\varphi = \theta_d * E_M \quad (3)$$

where θ_d and E_M are the number of valence electron and the electronegativity of the decorated TM, respectively (**Table S4**). As shown in **Figure 5(b)**, φ correlates linearly

with ε_d quite well, herein the results of the number of valence electrons multiplying by the electronegativity of the single atom is a descriptor to estimate the electronic structures and the potential performance of the SAC. Linear relationships were also found between θ_d and $E_b(N)$, as well as θ_d and φ, as shown in **Figures 5(c)** and **5(d)**. It is easy to deduce that the adsorption strength of N atom (*N) increases as the value of φ. Therefore, φ is a good descriptor to build a relationship between the basic characteristics of single TM atom and the adsorption energy of *N, as well as the electrocatalytic activity of NRR. Even without DFT calculation, it could be easily to find out the potential candidates with a relatively large value of φ. We looked into the connection between φ and the free energy changes of the critical steps of N_2 hydrogenation [$\Delta G(*NNH)$] and ammonia desorption [$\Delta G(*)$], and showed that results in **Figure 6**. The values are also linearly related to the descriptor φ for most SACs, except for the TM elements in Group IIIB and IVB. Furthermore, the elements with large φ have low free Gibbs energy changes for the two steps, such as Cu and Pt, consistent with the aforementioned assumption. Interestingly, the elements in Group IIIB and IVB, including Sc, Ti, Sc, Zr and Hf, do not follow the linear scaling relationship. They have small values of φ, but the corresponding SACs have low PDS energy change heights (< 0.70 eV, **Table 1**) as well. **Figure 3** shows that MoS_2 nanosheets decorated with these elements indeed feature thermodynamically stable *N species and demand huge amount of energy going from *N to $*NH_3$. On the other hand, their less than half filled *d*-orbitals form strong chemical bonds with nitrogen, thus the reductive hydrogenations of the following steps are all moderately endothermic. As a result, the overall energy increase is averaged, leading to three hydrogenation steps with similar and relatively low energy change. Such pattern has also been found in the chemisorption on many other metal surfaces.[66] Many catalysis systems suffer from high uphill energy change due to the limitation imposed by scaling relations.[49] Our calculations suggest that using the early transition metals may break such limitation in specific cases.

In experimental environment, HER is an unwanted competing reaction with respect

to NRR. Adsorbed protons would be reduced to H_2 at less negative potential, resulting in low NRR selectivity. Hydrogen on Sc-, Ti-, Cu-, Zr-, Hf-, and Pt-based SACs yields the adsorption energies of -1.36, -1.31, -0.57, -1.35, -1.33, and -0.86 eV, respectively, which are comparable with the values of N_2 on these SACs (as listed in **Table S5**), except for the well-known HER electrocatalyst Pt. The results suggest that neither H nor N_2 has the overwhelming superiority over its counterpart to be selectively adsorbed on the SACs. Besides, as considered to be a critical factor to evaluate the electrocatalytic performance, the limiting potential (U_L) is defined as the applied potential requiring all the steps on the considered process are exergonic and can be calculated by $U_L = -\Delta G_{max}/e$. As compared in **Figure 7**, the relationship between U_L(HER) and U_L(NRR) for the six candidate systems indicates that Sc, Ti, Zr and Hf should have remarkably higher NRR performance than HER, since the values of U_L(NRR) are much larger than that of U_L(HER). However, the single atom Cu decorated MoS_2 shows the selectivity towards HER, since its U_L(NRR) is much lower than that of U_L(HER), while Pt doesn't show its selectivity towards HER or NRR via the criterion U_L. Taking the solvation into consideration, the results shown in **Figure S4** confirm the high selectivity towards NRR for Sc-, Ti-, Zr- and Hf-decorated MoS_2 systems.

Conclusions

In summary, based on DFT calculations, we demonstrated that the defective MoS_2 decorated with single TM atom could be a promising electrochemical catalyst for ammonia synthesis at room temperature. Our systematically screening of a series of TM elements suggested that the embedded TM alters the substrate's electronic structures, facilitating the polarization and activation of the inert N_2 molecule. The computed free energy profiles show that the binding between nitrogen and decorated metal is so strong that the reductive hydrogenation and desorption of the second ammonia molecule limit the overall NRR process. Ti-decorated system has the lowest

PDS energy change of 0.63 eV, and the nanosheets decorated with Sc, Cu, Zr, Hf, and Pt also possess the energy change of lower that 0.70 eV. These materials are considered as the most promising electrocatalysts. To give a general view of the catalytic capacity, we studied the relationship between the center of the *d*-orbital of the decorated metal and the binding strength to nitrogen. A descriptor φ is introduced, which correlates linearly with the *d*-band center of the decorated atoms as well as the binding energy of nitrogen. Most metals with large values of φ, namely weak bonding to nitrogen, have relatively low energy changes of PDS, except those in Group IIIB and IVB. Although it is extremely endothermic from *N intermediate to desorbed NH_3, the half-filed *d*-orbital averages the free energy changes of the three steps of reductive hydrogenations, leading to a relatively low energy height of PDS. Therefore, decorating with the elements in Group IIIB and IVB may be an effective strategy to overcome the scaling relationship. Moreover, we also looked into the HER process of the candidate systems, and found that those defective MoS_2 decorated with Sc, Ti, Zr and Hf are indeed the most efficient and selective electrocatalysts for NRR in our screened SACs.

Supporting Information

ero point energies and entropy of different adsorption species, density of states profiles of all decorated species, binding energy of different TM atoms, free energy profiles of NRR processes for remaining species, adsorption energy of N_2 molecule, binding energy to nitrogen and *d*-band center of different TM atoms, valance electron in *d*-orbital, electronegativity of TM atoms, and coordinates of geometric structures.

Author Contributions

# H. G. and L.L. contributed equally.

Acknowledgments

This work was supported by the National Key Research and Development Program of China (No. 2018YFB0704300), the National Science Foundation of China (No. 21803074), the China Postdoctoral Science Foundation (No.2019T12832), NingBo S&T Innovation 2025 Major Special Program (No. 2018B10016), the program for Ningbo municipal science and technology innovative research team (2015B11002) and Fujian Institute of Innovation, Chinese Academy of Sciences. H.Y. is the recipient of an Australian Research Council Future Fellowship (Project number FT110100034) and X.W. is the recipient of the University of Wollongong Vice-Chancellor's Postdoctoral Research Fellowship. This research used computational resources of the High-Performance Computing Center of Collaborative Innovation Center of Advanced Microstructures, Nanjing University.

References

(1) Grunze, M. Synthesis and decomposition of ammonia. The Chemical Physics of Solid Surfaces and Heterogeneous Catalysis. *Elsevier scientific publishing company:* **1982**; Vol. 4.

(2) Jennings; Richard, J. Catalytic Ammonia Synthesis: Fundamentals and Practice. *Springer Science & Business Media:* **2013**.

(3) Erisman, J. W.; Sutton, M. A.; Galloway J.; Klimont, Z.; Winiwarter, W. How a Century of Ammonia Synthesis Changed the World. *Nat. Geosci.* **2008**, 1, 636-639.

(4) Christensen, C. H.; Johannessen, T.; Sørensen, R. Z.; Nørskov, J. K. Towards an Ammonia-Mediated Hydrogen Economy? *Catal. Today.* **2006**, 111, 140-144.

(5) Guo, J.; Chen, P. Catalyst: NH_3 as an Energy Carrier. *Chem.* **2017**, 3, 709-714.

(6) Van Der Ham, C. J. M.; Koper, M. T. M.; Hetterscheid, D. G. H. Challenges in Reduction of Dinitrogen by Proton and Electron Transfer. *Chem. Soc. Rev.* **2014**, 43, 5183-5191.

(7) Chen, G. F.; Ren, S.; Zhang, L.; Cheng, H.; Luo, Y.; Zhu, K.; Ding, L. X.; Wang, H. Advances in Electrocatalytic N_2 Reduction-Strategies to Tackle the Selectivity Challenge. *Small Methods* **2018**, 1800337.

(8) Chen, G. F.; Cao, X.; Wu, S.; Zeng, X.; Ding, L. X.; Zhu, M.; Wang, H. Ammonia Electrosynthesis with High Selectivity Under Ambient Conditions via a Li^+ Incorporation Strategy. *J. Am. Chem. Soc.* **2017**, 139, 9771-9774.

(9) Bao, D.; Zhang, Q.; Meng, F. L.; Zhong, H. X.; Shi, M. M.; Zhang, Y.; Yan, J. M.; Jiang, Q.; Zhang, X. B. Electrochemical Reduction of N_2 Under Ambient Conditions for Artificial N_2 Fixation and Renewable Energy Storage Using N_2/NH_3 Cycle. *Adv. Mater.* **2017**, 29, 1604799.

(10) Zhou, F.; Azofra, L. M.; Ali, M.; Kar, M.; Simonov, A. N.; Mcdonnell-Worth, C.; Sun, C.; Zhang, X.; Macfarlane, D. R. Electro-Synthesis of Ammonia From Nitrogen at Ambient Temperature and Pressure in Ionic Liquids. *Energy Environ. Sci.* **2017**, 10, 2516-2520.

(11) Shi, M. M.; Bao, D.; Wulan, B. R.; Li, Y. H.; Zhang, Y. F.; Yan, J. M.; Jiang, Q. Au Sub-Nanoclusters on TiO_2 toward Highly Efficient and Selective Electrocatalyst for N_2 Conversion to NH_3 at Ambient Conditions. *Adv. Mater.* **2017**, 29, 1606550.

(12) Chen, S.; Perathoner, S.; Ampelli, C.; Mebrahtu, C.; Su, D.; Centi, G. Electrocatalytic Synthesis of Ammonia at Room Temperature and Atmospheric Pressure from Water and Nitrogen on a Carbon-Nanotube-Based Electrocatalyst. *Angew. Chem. Int. Ed.* **2017**, 56, 2699-2703.

(13) Shi, M. M.; Bao, D.; Li, S. J.; Wulan, B. R.; Yan, J. M.; Jiang, Q. Anchoring PdCu Amorphous Nanocluster on Graphene for Electrochemical Reduction of N_2 to NH_3 under Ambient Conditions in Aqueous Solution. *Adv. Energy Mater.* **2018**, 8, 1800124.

(14) Liu, Y.; Su, Y.; Quan, X.; Fan, X.; Chen, S.; Yu, H.; Zhao, H.; Zhang, Y.; Zhao, J. Facile Ammonia Synthesis from Electrocatalytic N_2 Reduction under Ambient Conditions on N-Doped Porous Carbon. *ACS Catal.* **2018**, 8, 1186-1191.

(15) Zhang, L.; Ji, X.; Ren, X.; Ma, Y.; Shi, X.; Tian, Z.; Asiri, A. M.; Chen, L.; Tang, B.; Sun, X. Electrochemical Ammonia Synthesis via Nitrogen Reduction Reaction on a MoS_2 Catalyst: Theoretical and Experimental Studies. *Adv. Mater.* **2018**, 30, 1800191.

(16) Li, X.; Li, T.; Ma, Y.; Wei, Q.; Qiu, W.; Guo, H.; Shi, X.; Zhang, P.; Asiri, A. M.; Chen, L.; Tang, B.; Sun, X. Boosted Electrocatalytic N_2 Reduction to NH_3 by Defect-Rich MoS_2 Nanoflower. *Adv. Energy Mater.* **2018**, 8, 1801357.

(17) Andersen, S. Z.; Colic, V.; Yang, S.; Schwalbe, J. A.; Nielander, A. C.; McEnaney, J. M.; Enemark-Rasmussen, K.; Baker, J. G.; Singh, A. R.; Rohr, B. A.; Statt, M. J.; Blair, S. J.; Mezzavilla, S.; Kibsgaard, J.; Vesborg, P. C. K.; Cargnello, M.; Bent, S. F.; Jaramillo, T. F.; Stephens, I. E. L.; Norskov, J. K.; Chorkendorff, I. A Rigorous Electrochemical Ammonia Synthesis Protocol with Quantitative Isotope Measurements. *Nature* **2019**, 570, 504-508.

(18) Skulason, E.; Bligaard, T.; Gudmundsdottir, S.; Studt, F.; Rossmeisl, J.; Abild-Pedersen, F.; Vegge, T.; Jonsson, H.; Norskov, J. K. A Theoretical Evaluation of Possible Transition Metal Electro-Catalysts for N_2 Reduction. *Phys. Chem. Chem. Phys.* **2012**, 14, 1235-1245.

(19) Abghoui, Y.; Garden, A. L.; Howalt, J. G.; Vegge, T.; Skúlason, E. Electroreduction of N_2 to Ammonia at Ambient Conditions on Mononitrides of Zr, Nb, Cr, and V: A DFT Guide for Experiments. *ACS Catal.* **2015**, 6, 635-646.

(20) Li, X. F.; Li, Q. K.; Cheng, J.; Liu, L.; Yan, Q.; Wu, Y.; Zhang, X. H.; Wang, Z. Y.;

Qiu, Q.; Luo, Y. Conversion of Dinitrogen to Ammonia by FeN_3-Embedded Graphene. *J. Am. Chem. Soc.* **2016**, 138, 8706-8709.

(21) Macleod, K. C.; Mcwilliams, S. F.; Mercado, B. Q.; Holland, P. L. Stepwise N–H Bond Formation from N_2-Derived Iron Nitride, Imide and Amide Intermediates to Ammonia. *Chem. Sci.* **2016**, 7, 5736-5746.

(22) Azofra, L. M.; Li, N.; Macfarlane, D. R.; Sun, C. Promising Prospects for 2D d^2–d^4 M_3C_2 Transition Metal Carbides (MXenes) in N_2 Capture and Conversion into Ammonia. *Energy Environ. Sci.* **2016**, 9, 2545-2549.

(23) Zhao, J.; Chen, Z. Single Mo Atom Supported on Defective Boron Nitride Monolayer as an Efficient Electrocatalyst for Nitrogen Fixation: A Computational Study. *J. Am. Chem. Soc.* **2017**, 139, 12480-12487.

(24) Li, Q.; He, L.; Sun, C.; Zhang, X. Computational Study of MoN_2 Monolayer as Electrochemical Catalysts for Nitrogen Reduction. *J. Phys. Chem. C* **2017**, 121, 27563-27568.

(25) Abghoui, Y.; Skúlason, E. Onset Potentials for Different Reaction Mechanisms of Nitrogen Activation to Ammonia on Transition Metal Nitride Electro-Catalysts. *Catal. Today* **2017**, 286, 69-77.

(26) Ling, C.; Niu, X.; Li, Q.; Du, A.; Wang, J. Metal-Free Single Atom Catalyst for N_2 Fixation Driven by Visible Light. *J. Am. Chem. Soc.* **2018**, 140, 14161-14168.

(27) Wei, Z.; Zhang, Y.; Wang, S.; Ma, J. Fe-Doped Phosphorene for the Nitrogen Reduction Reaction. *J. Mater. Chem. A* **2018**, 6, 13790–13796.

(28) Zhang, L.; Sharada, S. M.; Singh, A. R.; Rohr, B. A.; Su, Y.; Qiao, L.; Nørskov, J. K. A Theoretical Study of the Effect of a Non-Aqueous Proton Donor on Electrochemical Ammonia Synthesis. *Phys. Chem. Chem. Phys.* **2018**, 20, 4982-4989.

(29) Ling, C.; Bai, X.; Ouyang, Y.; Du, A.; Wang, J. Single Molybdenum Atom Anchored on N-Doped Carbon as a Promising Electrocatalyst for Nitrogen Reduction into Ammonia at Ambient Conditions. *J. Phys. Chem. C* **2018**, 122, 16842-16847.

(30) Cao, Y.; Gao, Y.; Zhou, H.; Chen, X.; Hu, H.; Deng, S.; Zhong, X.; Zhuang, G.; Wang, J. Highly Efficient Ammonia Synthesis Electrocatalyst: Single Ru Atom on Naturally Nanoporous Carbon Materials. *Adv. Theory Simul.* **2018**, 1, 1800018.

(31) Qiao, B.; Wang, A.; Yang, X.; Allard, L. F.; Jiang, Z.; Cui, Y.; Liu, J.; Li, J.; Zhang, T. Single-Atom Catalysis of CO Oxidation Using Pt_1/FeO_x. *Nat. Chem.* **2011**, 3, 634-641.

(32) Bayatsarmadi, B.; Zheng, Y.; Vasileff, A.; Qiao, S. Z. Recent Advances in Atomic Metal Doping of Carbon-based Nanomaterials for Energy Conversion. *Small* **2017**, 13, 1700191.

(33) Xu, H.; Cheng, D.; Cao, D.; Zeng, X. C. A Universal Principle for a Rational Design of Single-Atom Electrocatalysts. *Nat. Catal.* **2018**, 1, 339-348.

(34) Qiu, H. J.; Ito, Y.; Cong, W.; Tan, Y.; Liu, P.; Hirata, A.; Fujita, T.; Tang, Z.; Chen, M. Nanoporous Graphene with Single-Atom Nickel Dopants: An Efficient and Stable Catalyst for Electrochemical Hydrogen Production. *Angew. Chem. Int. Ed.* **2015**, 54, 14031-14035.

(35) Bulushev, D. A.; Zacharska, M.; Lisitsyn, A. S.; Podyacheva, O. Y.; Hage, F. S.; Ramasse, Q. M.; Bangert, U.; Bulusheva, L. G. Single Atoms of Pt-Group Metals Stabilized by N-Doped Carbon Nanofibers for Efficient Hydrogen Production from Formic Acid. *ACS Catal.* **2016**, 6, 3442-3451.

(36) Calle-Vallejo, F.; Tymoczko, J.; Colic, V.; Vu, Q. H.; Pohl, M. D.; Morgenstern, K.; Loffreda, D.; Sautet, P.; Schuhmann, W.; Bandarenka, A. S. Finding Optimal Surface Sites on Heterogeneous Catalysts by Counting Nearest Neighbors. *Science* **2015**, 350, 185-189.

(37) Yin, P.; Yao, T.; Wu, Y.; Zheng, L.; Lin, Y.; Liu, W.; Ju, H.; Zhu, J.; Hong, X.; Deng, Z.; Zhou, G.; Wei, S.; Li, Y. Single Cobalt Atoms with Precise N-Coordination as Superior Oxygen Reduction Reaction Catalysts. *Angew. Chem. Int. Ed.* **2016**, 55, 10800-10805.

(38) Yang, S.; Tak, Y. J.; Kim, J.; Soon, A.; Lee, H. Support Effects in Single-Atom Platinum Catalysts for Electrochemical Oxygen Reduction. *ACS Catal.* **2016**, 7, 1301−1307.

(39) Li, X.; Cui, P.; Zhong, W.; Li, J.; Wang, X.; Wang, Z.; Jiang, J. Graphitic Carbon Nitride Supported Single-Atom Catalysts for Efficient Oxygen Evolution Reaction. *Chem. Commun.* **2016**, 52, 13233-13236.

(40) Wurster, B.; Grumelli, D.; Hotger, D.; Gutzler, R.; Kern, K. Driving the Oxygen Evolution Reaction by Nonlinear Cooperativity in Bimetallic Coordination Catalysts. *J. Am. Chem. Soc.* **2016**, 138, 3623-3626.

(41) Geng, Z.; Liu, Y.; Kong, X.; Li, P.; Li, K.; Liu, Z.; Du, J.; Shu, M.; Si, R.; Zeng, J.

Achieving a Record-High Yield Rate of 120.9 μg_{NH3} $mg_{cat.}^{-1}$ h^{-1} for N_2 Electrochemical Reduction over Ru Single-Atom Catalysts. *Adv. Mater.* **2018**, 30, 1803498.

(42) Gao, Y.; Cai, Z.; Wu, X.; Lv, Z.; Wu, P.; Cai, C. Graphdiyne-Supported Single-Atom-Sized Fe Catalysts for the Oxygen Reduction Reaction: DFT Predictions and Experimental Validations. *ACS Catal.* **2018**, 8, 10364-10374.

(43) Peng, Y.; Lu, B.; Chen, S. Carbon-Supported Single Atom Catalysts for Electrochemical Energy Conversion and Storage. *Adv. Mater.* **2018**, 30, 1801995.

(44) Azofra, L. M.; Sun, C.; Cavallo, L.; MacFarlane, D. R. Feasibility of N_2 Binding and Reduction to Ammonia on Fe-Deposited MoS_2 2D Sheets: A DFT Study. *Chem. Eur. J.* 2017, 23, 8275-8279.

(45) Ling, C.; Niu, X.; Li, Q.; Du, A.; Wang, J. Metal-Free Single Atom Catalyst for N_2 Fixation Driven by Visible Light. *J. Am. Chem. Soc.* **2018**, 140, 14161-14168.

(46) Wang, Z.; Yu, Z.; Zhao, J. Computational Screening of a Single Transition Metal Atom Supported on the C_2N Monolayer for Electrochemical Ammonia Synthesis. *Phys. Chem. Chem. Phys.* **2018**, 20, 12835-12844.

(47) Hinnemann, B.; Moses, P. G.; Bonde, J.; Jørgensen, K. P.; Nielsen, J. H.; Horch, S.; Chorkendorff, I.; Nørskov, J. K. Biomimetic Hydrogen Evolution: MoS_2 Nanoparticles as Catalyst for Hydrogen Evolution. *J. Am. Chem. Soc.* **2005**, 127, 5308-5309.

(48) Jaramillo, T. F.; Jørgensen, K. P.; Bonde, J.; Nielsen, J. H.; Horch, S.; Chorkendorff, I. Identification of Active Edge Sites for Electrochemical H_2 Evolution from MoS_2 Nanocatalysts. *Science* **2007**, 317, 100-102.

(49) Li, Y.; Sun, Q. Recent Advances in Breaking Scaling Relations for Effective Electrochemical Conversion of CO_2. *Adv. Energy Mater.* **2016**, 6, 1600463.

(50) Kresse, G.; Hafner, J. Ab Initio Molecular-Dynamics Simulation of the Liquid-Metal-Amorphous-Semiconductor Transition in Germanium. *Phys. Rev. B* **1994**, 49, 14251-14269.

(51) Kresse, G. Efficient Iterative Schemes for Ab Initio Total-Energy Calculations Using a Plane-Wave Basis Set. *Phys. Rev. B* **1996**, 54, 11169-11186.

(52) Kresse, G.; Furthmüller, J. Efficiency of ab-initio Total Energy Calculations for Metals and Semiconductors Using a Plane-Wave Basis Set. *Comp. Mater. Sci.* **1996**, 6, 15-50.

(53) Segall, M. D.; Lindan, P. J. D.; Probert, M. J.; Pickard, C. J.; Hasnip, P. J.; Clark, S. J.; Payne, M. C. First-Principles Simulation: Ideas, Illustrations and the CASTEP Code. *J. Phys.: Condens. Mat.* **2002**, 14, 2717-2744.

(54) Perdew, J. P. Atoms, molecules, solids, and surfaces: Applications of the Generalized Gradient Approximation for Exchange and Correlation. *Phys. Rev. B* **1992**, 46, 6671-6687.

(55) Blochl, P. E. Projector Augmented-Wave Method. *Phys. Rev. B* **1994**, 50, 17953-17979.

(56) Grimme, S.; Antony, J.; Ehrlich, S.; Krieg, H. A Consistent and Accurate Ab Initio Parametrization of Density Functional Dispersion Correction (DFT-D) for the 94 Elements H-Pu. *J. Chem. Phys.* **2010**, 132, 154104.

(57) Monkhorst, H. J.; Pack, J. D. Special Points for Brillonin-Zone Integrations. *Phys. Rev. B* **1976**, 13, 5188-5192.

(58) Zhao, J.; Zhao, J.; Cai, Q. Single Transition Metal Atom Embedded into a MoS_2 Nanosheet as a Promising Catalyst for Electrochemical Ammonia Synthesis. *Phys. Chem. Chem. Phys.* **2018**, 20, 9248-9255.

(59) Santosh, K.; Longo, R. C.; Addou, R.; Wallace, R. M.; Cho, K. Impact of Intrinsic Atomic Defects on the Electronic Structure of MoS_2 Monolayers. *Nanotechnology* **2014**, 25, 375703.

(60) Mathew, K.; Sundararaman, R.; Letchworth-Weaver, K.; Arias, T.; Hennig, R. G. Implicit Solvation Model for Density-Functional Study of Nanocrystal Surfaces and Reaction Pathways. *J. Chem. Phys.* **2014**, 140, 084106.

(61) Tomasi, J.; Mennucci, B.; Cammi, R. Quantum Mechanical Continuum Solvation Models. *Chem. Rev.* **2005**, 105, 2999-3094.

(62) Calle-Vallejo, F.; Inoglu, N. G.; Su, H.-Y.; Martínez, J. I.; Man, I. C.; Koper, M. T. M.; Kitchin, J. R.; Rossmeisl, J. Number of Outer Electrons as Descriptor for Adsorption Processes on Transition Metals and Their Oxides. *Chem. Sci.* **2013**, 4, 1245-1249.

(63) Su, H. Y.; Sun, K.; Wang, W. Q.; Zeng, Z.; Calle-Vallejo, F.; Li, W. X. Establishing and Understanding Adsorption–Energy Scaling Relations with Negative Slopes. *J. Phys. Chem. Lett.* **2016**, 7, 5302-5306.

(64) Calle-Vallejo, F.; Díaz-Morales, O. A.; Kolb, M. J.; Koper, M. T. M. Why Is Bulk Thermochemistry a Good Descriptor for the Electrocatalytic Activity of Transition Metal Oxides? *ACS Catal.* **2015**, 5, 869-873.

(65) Calle-Vallejo, F.; Martínez, J. I.; Rossmeisl, J. Density Functional Studies of Functionalized Graphitic Materials with Late Transition Metals for Oxygen Reduction Reactions. *Phys. Chem. Chem. Phys.* **2011**, 13, 15639-15643.

(66) Xin, H.; Linic, S. Communications: Exceptions to the *d*-band Model of Chemisorption on Metal Surfaces: The Dominant Role of Repulsion Between Adsorbate States and Metal *d*-states. *J. Chem. Phys.* **2010**, 132, 221101.

Figure and Tables

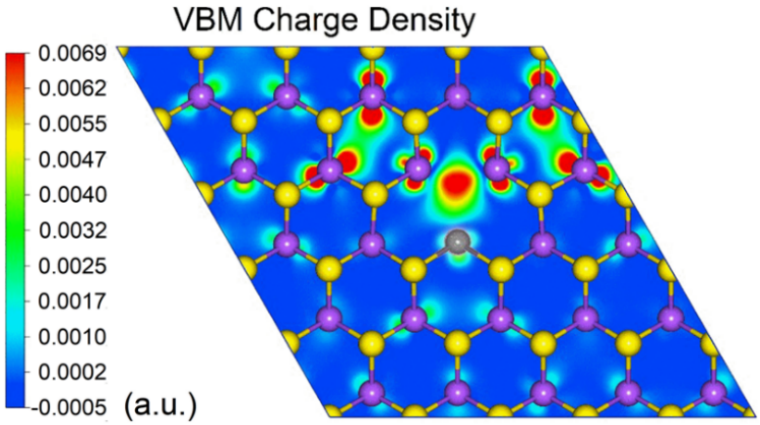

Figure 1. Top view of a typical decorated defective model. Color code: yellow, S; purple, Mo; grey, Sc alien atom. The background is the charge density difference of valence band in Sc-decorated defective MoS_2. Red and blue areas represent electron accumulation and depletion regions.

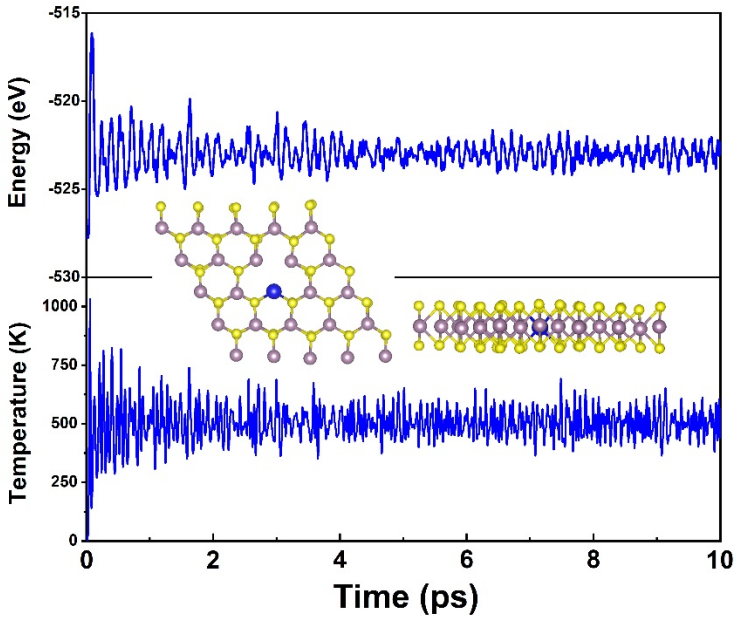

Figure 2. Variations of temperature and energy versus time for AIMD simulations of Sc-decorated defective MoS_2. Inset figures are the top and side views of relaxed structure.

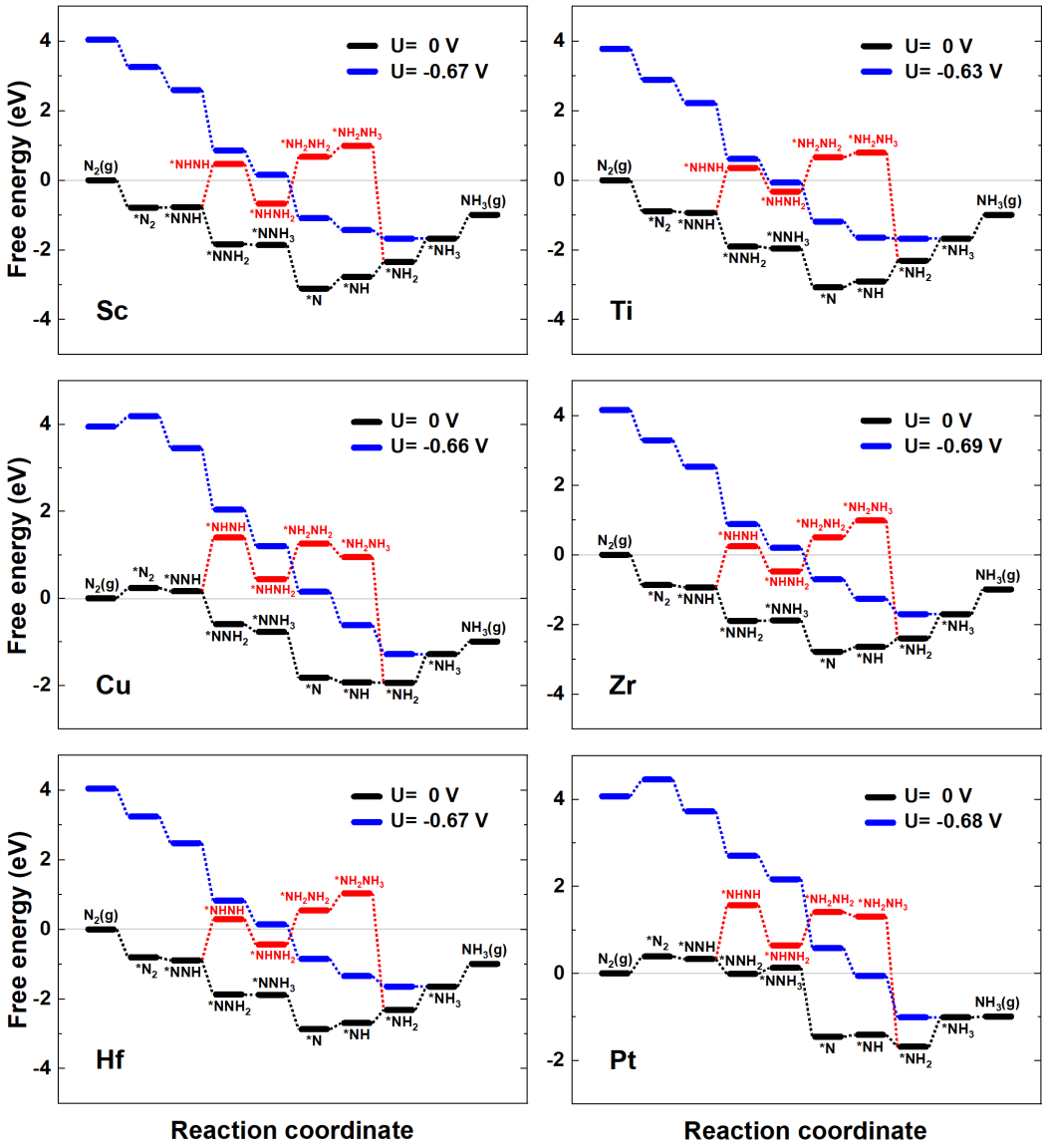

Figure 3. Free energy profiles of NRR processes without (black lines) and with applied potential (blue lines) through the distal mechanism. Red lines illustrate NRR processes via the alternating mechanism. The asterisk (*) denotes the adsorption site.

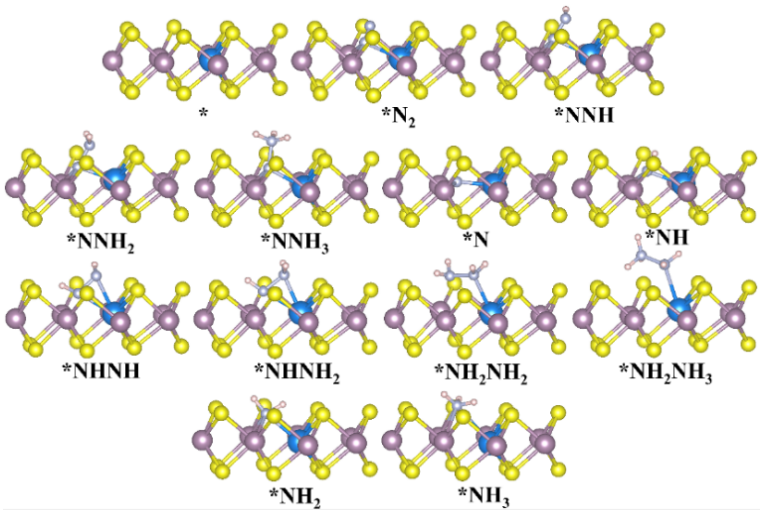

Figure 4. Typical structures of these species on the NRR pathways. The Sc-decorated species are taken as examples. The asterisk denotes to the adsorption site.

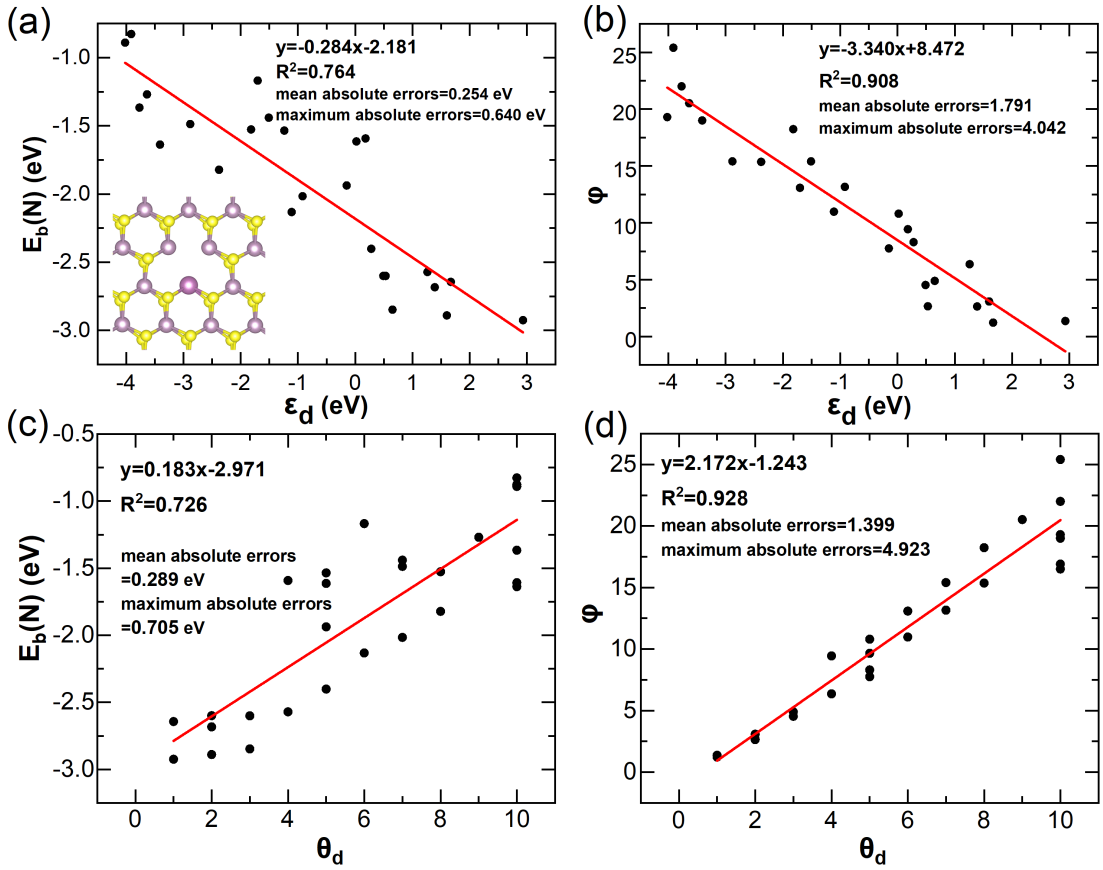

Figure 5. Linear relationships between (a) ε_d and $E_b(N)$, (b) φ and ε_d, (c) θ_d and $E_b(N)$, (d) θ_d and φ.

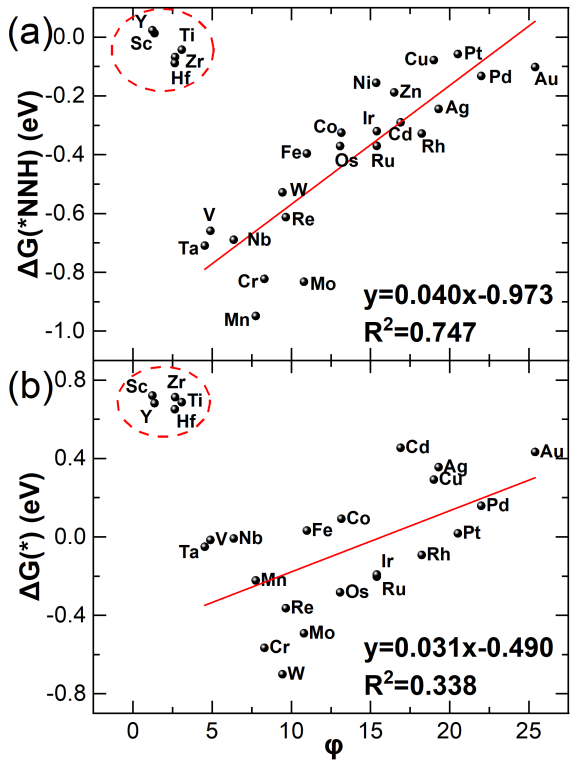

Figure 6. Relationships between (a) φ and ΔG(*NNH), (b) φ and ΔG(*). The outliers are highlighted in red circle. The mean and maximun absolute errors are 0.107, 0.291 eV for Fig. 6a and 0.227, 0.503 eV for Fig. 6b, respectively, expect Sc, Ti, Y, Zr, Hf.

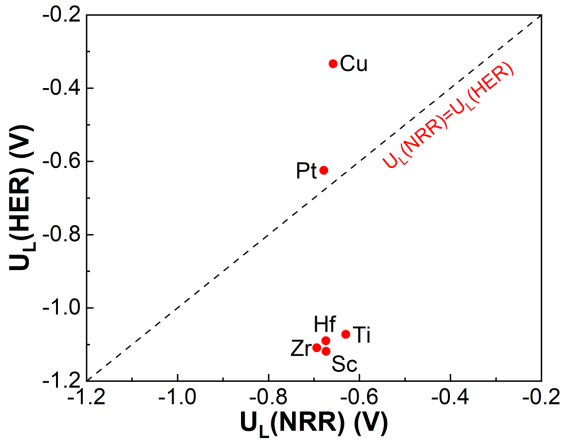

Figure 7. The limiting potentials of HER [U_L(HER)] versus NRR [U_L(NRR)] on various SACs. SACs in the region under the dashed line corresponds to NRR being more favorable than HER.

Table 1. Corresponding free energy changes of the PDS in the periodic table of elements. The elements with energy changes of PDS under 0.70 V, between 0.70 and 1.00 eV, and above 1.00 eV are marked in green, yellow, and red, respectively.

IIIB	IVB	VB	VIB	VIIB	VIIIB			IB	IIB
Sc 0.67	Ti 0.63	V 1.28	Cr 1.19	Mn 1.01	Fe 0.75	Co 0.84	Ni 0.72	Cu 0.66	Zn 0.74
Y 0.75	Zr 0.69	Nb 1.31	Mo 1.59	Tc	Ru 1.04	Rh 0.85	Pd 0.71	Ag 0.79	Cd 0.79
(La)	Hf 0.67	Ta 1.26	W 1.64	Re 1.76	Os 1.24	Ir 0.78	Pt 0.68	Au 0.72	Hg

TOC Figure

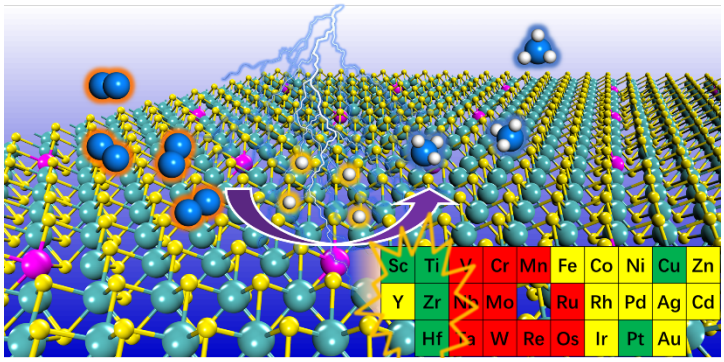
Sc Ti V Cr Mn Fe Co Ni Cu Zn
Y Zr Nb Mo Ru Rh Pd Ag Cd
Hf Ta W Re Os Ir Pt Au